Biosensors and Bioelectronics 74 (2015) 8–15

Contents lists available at ScienceDirect

Biosensors and Bioelectronics

journal homepage: www.elsevier.com/locate/bios

Kinetic studies of microfabricated biosensors using local adsorption strategy

Menglun Zhang, Jingze Huang, Weiwei Cui, Wei Pang, Hao Zhang*, Daihua Zhang, Xuexin Duan*

State Key Laboratory of Precision Measuring Technology & Instruments, College of Precision Instrument and Optoelectronics Engineering, Tianjin University, Tianjin 300072, China

ARTICLE INFO

Article history:
Received 4 April 2015
Received in revised form
22 May 2015
Accepted 26 May 2015
Available online 28 May 2015

Keywords:
Biosensor
Signal amplification
Local adsorption
Binding kinetics
FBAR

ABSTRACT

Micro/nano scale biosensors integrated with the local adsorption mask have been demonstrated to have a better limit of detection (*LOD*) and less sample consumptions. However, the molecular diffusions and binding kinetics in such confined droplet have been less studied which limited further development and application of the local adsorption method and imposed restrictions on discovery of new signal amplification strategies. In this work, we studied the kinetic issues via experimental investigations and theoretical analysis on microfabricated biosensors. Mass sensitive film bulk acoustic resonator (FBAR) sensors with hydrophobic Teflon film covering the non-sensing area as the mask were introduced. The fabricated masking sensors were characterized with physical adsorption of bovine serum albumin (BSA) and specific binding of antibody and antigen. Over an order of magnitude improvement on *LOD* was experimentally monitored. An analytical model was introduced to discuss the target molecule diffusion and binding kinetics in droplet environment, especially the crucial effects of incubation time, which has been less covered in previous local adsorption related literatures. An incubation time accumulated signal amplification effect was theoretically predicted, experimentally monitored and carefully explained. In addition, device optimization was explored based on the analytical model to fully utilize the merits of local adsorption. The discussions on the kinetic issues are believed to have wide implications for other types of micro/nano fabricated biosensors with potentially improved *LOD*.

1. Introduction

Highly sensitive biosensors which are able to detect trace quantities of biological analytes not only triggered a lot interests in the scientific research field but also are in great demand in medicine, agriculture, food safety, homeland security, environmental and industrial monitoring fields (Luong et al., 2008). Micro/nano scale biosensors (Xie et al., 2012; Yola et al., 2014; Zhang et al., 2013; Zhou et al., 2014) show great advantages to detect small amount of analytes which is partially due to their miniaturized device size, thus intrinsically consume less analytes. Besides, the high surface to volume ratio of such devices improves their sensitivity and the limit of detection (*LOD*) (Sheehan and Whitman, 2005). In conventional micro-fabricated biosensors, fluid networks (e.g. microfluidics) are usually integrated to deliver analytes to the sensor surface. However, it normally requires large amount of biosamples (more than 300 μl) to fill the whole networks and may lead to loss of precious bio-samples during their transport. Besides, such deliver method has less control in sample adsorption on the unwanted non-sensing area (e.g. sensor passivation area etc.). These drawbacks limit the real usage of such biosensors. In recent years, droplet or digital microfluidics combined with local adsorption techniques have opened new research directions to further reduce the required sample volume (less than 5 μl) (Bunimovich et al., 2004; Jebrail et al., 2012; Lee et al., 2003; Malic et al., 2010; Naujoks and Stemmer, 2003; Park et al., 2007; Renault et al., 2002; Whitesides, 2006), where unwanted target adsorption on the non-sensing area is blocked and target molecules only bind on the exposed sensing area (Choi et al., 2010; Ekins, 1998). Therefore, the microfabricated biosensors integrated with the local adsorption mask will have a larger signal response, and hence a better *LOD*. 10–100 fold enhancement of *LOD* has been reported in the literatures (Kim, C.H., et al., 2013; Kim, J.Y., et al., 2013; Lifson et al., 2014). In practice, due to the limited volume of sample droplets and the tiny binding area, the molecule diffusion in such small droplet and surface binding kinetics on the confined sensor area have to be optimized thus, the sample incubation time is an important factor. However, most of the previous studies are

* Corresponding authors.
E-mail addresses: haozhang@tju.edu.cn (H. Zhang), xduan@tju.edu.cn (X. Duan).

http://dx.doi.org/10.1016/j.bios.2015.05.061
0956-5663/

focused on the improvement of *LOD* and there are no detail studies on the kinetic issues of such local adsorption method in confined droplets.

In this work, we studied the kinetic issues of the masking local adsorption method using microfabricated film bulk acoustic resonators (FBARs). FBARs are known as excellent mass sensitive sensors and have been studied for many biological applications, including DNA hybridization (Nirschl et al., 2010; Zhang et al., 2007), protein detection (Nirschl et al., 2009; Zhang et al., 2010), and immunoassays (Wingqvist et al., 2007). Well-known Sauerbrey's equation (Sauerbrey, 1959) shows a linear relationship between the sensor signal and the mass loading on the sensing area. Compared with the conventional quartz crystal microbalance (QCM), micro-fabricated FBAR sensors have many inherent properties shared with microfluidic systems, such as small analyte consumption and compatible microfabrication process (Zhang et al., 2015). A thin film of hydrophobic Teflon is coated and patterned by the microfabrication process on top of the FBAR and covers the non-sensing area. The patterned Teflon functions as the mask, which prevents the adsorption of biomolecules. Two types of biomolecule interactions were compared experimentally using masking and non-masking FBAR sensors: 1) physical adsorption of BSA on type I FBAR sensor (Au film on top) and 2) anti-IgG specific interactions with IgG coated type II FBAR sensor (AlN film on top). An analytical model is introduced to analyze the target adsorption process. The incubation time together with the molecule diffusion and binding kinetics are carefully studied. In addition, device design has been optimized to exploit the merits of the masking method. Although other biosensors are topographically distinct, the rule on the kinetic issues will work equally with many microscale and nanoscale biosensors.

2. Material and methods

2.1. Reagents and materials

Bovine serum albumin (BSA) was purchased from Takara Bio (Japan). FITC-conjugated BSA was purchased from Sangon Biotech (Shanghai, China). Mouse IgG and quantum dots (QDs) labeled goat anti-mouse IgG were purchased from NNCrystal (Hangzhou, China). (3-Aminopropyl)triethoxysilane (APTES) was obtained from Aladdin (USA). 1,4-phenylene diisothiocyanate (PDC) was obtained from J&K Scientific (Beijing, China). Pluronic F127 was purchased from Fanbo Biochemicals (Beijing, China). Teflon AF 1600 was purchased from DuPont (USA). All other chemicals used were of analytical reagent grade. In order to prepare different concentrations of solutions, 10-fold serial dilutions were conducted on 0.1% (~15 μM) BSA solution, 1 mg/mL mouse IgG solution and 1 μM QDs labeled goat anti-mouse IgG solution with PBS solutions (1×, pH=7.4).

2.2. Device fabrication

The fabrication process of the Teflon masking prototype is described below. An air cavity was first formed in silicon substrate by reactive ion etching. Then the air cavity was filled with phosphosilicate glass (PSG). A 500 nm molybdenum (Mo), 1000 nm AlN, and 500 nm Mo were sequentially deposited and patterned on the substrate as the bottom electrode, piezoelectric film and top electrode, respectively. A 10 nm/80 nm Cr/Au composite film (type I) or 200 nm AlN film (type II) was then deposited and patterned to cover the whole sensing area. The silicon wafer was immersed in diluted hydrofluoric (HF) acid solution to remove PSG in the cavity. Finally a 30 nm Teflon film was spin-coated and patterned by a lift-off process to expose the sensing area.

2.3. Sensor surface functionalization

FBAR sensor was first cleaned by acetone, isopropyl alcohol, and deionized (DI) water sequentially before any functionalization. The surface of a type II sensor was cleaned with piranha. Then APTES was allowed to evaporate onto the sensor surface through gas phase deposition in a heated vacuum chamber (YES LabKote) for 15 mins (125 °C, 5.7 Torr). Transformation of the amino-terminated layer to an isothiocyanate-bearing layer was accomplished by exposure to PDC solution of 0.01 M in ethanol at 65 °C for 1 h, followed by rinsing with copious amounts of ethanol, DI water sequentially, and drying in compressed nitrogen gas. Then a 1.5 μL mouse IgG droplet was loaded on the device surface and covered the entire sensing area for 30 min. Afterward, Pluronic F127 of 1.6 mg/mL was coated on the Teflon mask to further prevent slight nonspecific target adsorption on the mask.

2.4. Protein sensing experiments

The whole sensing experiment procedures were carried out in the cleanroom. During the incubation, environmental interferences were minimized. Temperature was kept at around 20 °C. For long time incubation, devices were placed in a humidity chamber to prevent the droplet evaporation. For fair comparison, Teflon masking sensors and non-masking sensors (control group) were measured using the same experimental procedures.

After device surface modifications, the FBAR sensor was subjected to the first electrical testing. The series resonant frequency signal was obtained by a network analyzer (Agilent E5061B). The target droplet (typical 3–4 μl) was then loaded on the sensor surface to cover the whole sensing area. After a setting time, the protein droplet was removed, rinsed thoroughly with buffer and dried in compressed nitrogen gas. Finally, the FBAR sensor was subjected to the second electrical testing.

The sensor signal is defined as the shift between FBAR's resonant frequencies obtained from the two electrical tests. Minimum detectable frequency shift f was experimentally determined to obtain the *LOD* of the sensor system. *LOD* is defined at the target concentration of which solution causes the resonant frequency of a FBAR sensor to shift Δf. Δf is calculated by (Loock and Wentzell, 2012)

$$\Delta f = \bar{\Delta f_0} + 3 \times SD_f \tag{1}$$

where $\overline{\Delta f_0}$ and SD_f are the average frequency shift and standard deviation of repeated measurements of the blank samples, respectively. Blank sample detection was carried out by recording the frequency shift of an FBAR sensor caused by the rinsing step.

A fluorescent microscope (Olympus BX 53) was used to quantify the fluorescence labeled proteins on surface. The fluorescence intensity was acquired by a CCD camera. The exposure time and magnification were kept constant at 1 s and 20×. Data analysis was processed by Image-Pro Plus. To quantify the fluorescence data, the relative fluorescence intensity *RFI* is employed to measure the relative intensity boost of the Teflon masking to non-masking sensors, which is given by

$$RFI = \left(\frac{I_t - I_c}{I_n - I_c} - 1\right) \times 100\% \tag{2}$$

where I_c is the fluorescence intensity before target incubation as a control, and I_t and I_n are the Teflon masking and non-masking fluorescence intensities after target incubation, respectively.

3. Results and discussion

3.1. Devices

The schematic illustration of the Teflon masking FBAR sensor is shown in Fig. 1a. A typical FBAR comprises a piezoelectric layer, top and bottom electrodes, and an air cavity beneath the electrode/piezoelectric/electrode sandwiched structure (Pang et al., 2012). The sensing area is the surface of the active region, which is defined by the overlap region of the air cavity and the sandwiched structure. Hydrophobic Teflon film is patterned on the sensor surface to expose the active sensing area. The sensing area can be further functionalized with different bioreceptors for target detection.

A micrograph of a fabricated prototype FBAR sensor (type I) with Teflon masking is shown in Fig. 1b. Five microscale holes around the sensing area are used to facilitate releasing of the sacrificial material. Besides functioning as the mask, Teflon film is coated inside the holes as well to prevent liquid getting into the air cavities which will increase the sensor stability in liquid environment. The ground-signal-ground (GSG) pads connect the sensing area of the FBAR sensor to extract electrical signal. Non-masking FBAR sensor (control groups) has identical structure and top electrodes except for the absence of the Teflon film on top.

3.2. Protein sensing result

BSA exhibits common physical properties of proteins and would physically adsorb on many sensor surface without additional surface functionalization. A number of works have used BSA as target analytes to evaluate the sensors performance for protein detections (Kim, E., et al., 2013; Moulin et al., 1999; Nakata et al., 1996; Silin et al., 1997; Wingqvist et al., 2009). A BSA adsorption process may clearly reveal the kinetic course in this research by eliminating the interference of imperfect surface modification. In order to characterize the signal amplification quantitatively, Au coated FBAR (type I) sensors are applied to measure the adsorption of BSA. FITC-conjugated BSA is also employed in fluorescence detection to qualitatively confirm the amplification effect. For optical measurement, the Au film in type I sensor is replaced by a silicon oxide film to prevent the Au quenching effect and facilitate the fluorescence observation.

Besides the physical adsorption, we also studied the protein specific interaction using masking FBAR sensors. Unlike BSA adsorption, goat anti-mouse IgGs would specifically bind with mouse IgGs. Here, goat anti-mouse IgG is employed as the target of the type II sensor. After IgG covalent immobilization on FBAR, the sensor is incubated with the anti-IgG target droplet. As a comparison, QDs labeled goat anti-mouse IgG solutions are used in fluorescence demonstration. In both BSA and anti-IgG detections, the diluted target droplets could be easily loaded on and removed off from the FBAR surface, which benefits from the rather large hydrophobic coating on the non-sensing area.

The electrical detection signal of a FBAR sensor is expressed as shift of the resonant frequency, which is derived by the zero-reactance method, due to a higher detection precision than tracking the minimum point of impedance magnitude (Zhang and Kim, 2005). According to the reactance curves of the FBAR sensor before and after incubation in a BSA droplet of 150 nM, a sensor signal of −53 kHz is calculated, as shown in Fig. S1. In this way, signals of the masking and non-masking sensors are recorded and compared for each target concentration.

For both BSA and anti-IgG detections, the fluorescence intensity in the sensing areas is visibly higher with the Teflon masking (Fig. S2), which preliminarily demonstrates the signal amplification effect. The *RFI* value in Fig. 2a shows that the fluorescence intensity of a Teflon masking substrate is 160% higher than that of the non-masking substrate when incubated in BSA droplets of 1.5 μM. However, there is no distinct fluorescence intensity difference between the masking and non-masking substrates when incubated with higher BSA concentration (15 μM). To better quantify the results, we tested the 15 μM BSA droplets using masking and non-masking FBAR sensors with different incubation times (Fig. 2b). The results show that the frequency shifts are almost the same between the two devices even after incubating for 40 min, indicating that the masking method is less effective with high concentration samples. This is likely due to the reason that the sensor surface is easily saturated with the rather high protein concentrations; thus the surface depletion will not happen in this case and the signal amplification is less effective.

From these results, the signal amplification effect by the masking method should be more pronounced at lower sample concentrations. However, a fluorescence technique is difficult to measure protein concentrations less than 1.5 μM; thus we applied masking FBAR sensors to detect low protein concentrations down to nanomolar. As shown in Fig. 3, the sensor responses of the Teflon masking sensor are always larger than the non-masking ones in low protein concentration range with both BSA physical adsorption and anti-IgG specific bindings. The larger signals on Teflon masking sensor over the control group at various concentrations clearly confirm the amplification effect and prove our hypothesis.

In both BSA and anti-IgG detections, the *LODs* of masking and non-masking FBAR sensors are compared. The absolute value of minimum detectable frequency shift (device noise) is around 8 kHz. Fig. 3a shows that the signal of 15 nM BSA measuring from the non-masking sensor is below the device noise, while the Teflon masking sensor shows a significant frequency shift under the same conditions. The *LOD* of a Teflon masking FBAR sensor for BSA detection is roughly 1.5 nM. Anti-IgG detections show similar results at 1 nM (Fig. 3b). Therefore, the *LOD* of an FBAR sensor is experimentally found to be improved by at least an order of

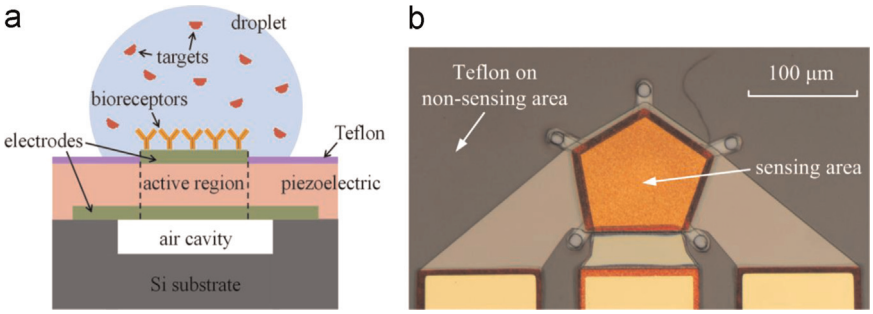

Fig. 1. (a) Schematic illustration (cross-sectional view) of the Teflon masking FBAR sensor. Note that bioreceptors are optional. (b) Microscopic photograph (top view) of a fabricated type I FBAR sensor with Teflon masking. The sensing area is a pentagon with a length of about 100 μm.

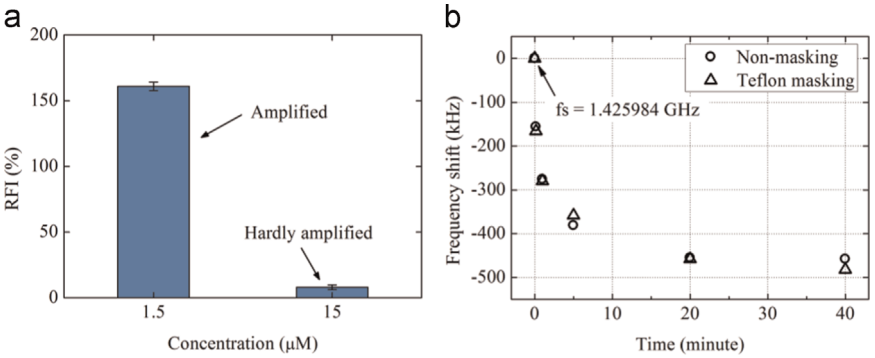

Fig. 2. (a) BSA fluorescence detection result (relative fluorescence intensity) at 15 μM and 1.5 μM. Error bars are calculated from standard deviations of relative fluorescence intensities. The incubation time is 20 min. (b) Electrical detection signal of FBAR sensors incubated in BSA target droplets of 15 μM at various incubation time.

magnitude by the Teflon masking method.

3.3. Kinetic issues

In order to give a deeper insight into the signal amplification mechanism, the kinetic issues of the masking method are studied. Signal amplifications measuring from FBAR sensors at different incubation times are recorded. An analytical model considering the molecular diffusion and binding kinetics in droplet confined condition is applied to analyze the data. A numerical model is also built to validate the analysis.

3.3.1. Numerical model

A Finite element method (FEM) is adopted to analyze the two adsorption schemes. The numerical solutions are derived by modeling in COMSOL Multiphysics 3.5a. We apply transit analyses on the diffusion module, and simplify the device geometry to a 2D axial symmetry due to device symmetry, as shown in Fig. 4c and d. The shape of a droplet on the device surface is a section of a sphere. The droplet on the non-masking device tends to spread on the hydrophilic AlN surface which has a contact angle (CA) of 59°; the droplet on the Teflon masking device "stands up" on the hydrophobic Teflon surface, where CA is 129°, as shown in Fig. 4a and b. With the measured CAs, the geometry of the droplet in each adsorption scheme can be accurately modeled in FEM simulation. Since the sensing area is relatively small compared with the droplet in size, the mesh is finer in the vicinity of the device surface.

Before the adsorption process, the droplet contains a uniformly distributed target molecules and the device surface is empty. The target–receptor binding stoichiometry is assumed to be 1:1 and the receptors on the device surface formed a monolayer; thus the classic Langmuir binding kinetic can be applied to descript the target–receptor binding process (Georgiadis et al., 2000). In the non-masking scheme, the consumption rates of target molecules on the sensing area and non-sensing area are equal, which leads to a roughly uniform-distributed depletion layer. Therefore the molecules away from the device surface diffuse vertically as shown in Fig. 4e. In the Teflon masking scheme, hydrophobic Teflon surface repulses water thus, the target molecules only adsorb to the sensing area, which creates a sensing area-centered hemispheric depletion layer as shown in Fig. 4f.

3.3.2. Analytical model

In the analytical model, the physical settings and assumptions are the same with the numerical model. The adsorption rate of target molecules on the receptor surface is calculated as

$$\frac{dc_s}{dt} = k_{on} \times c \times (\theta_{max} - c_s) - k_{off} \times c_s \tag{3}$$

where c_s is the surface concentration of bounded target, t is the incubation time, c is the bulk concentration of target, θ_{max} is maximum surface concentration of receptor sites, k_{on} and k_{off} are the association and dissociation rate constant for a target–receptor binding pair. k_{off} is normally very small in BSA physical adsorption and high affinity protein binding systems; thus we simplified Eq. (3) by taking off k_{off} (Nair and Alam, 2006). With the excellent approximation, c_s can be derived by balancing between the incident flux and the target–receptor binding flux as

$$c_s = c_0 \times t \times \left(\frac{A_D}{C_D(t)} + \frac{1}{k_{on} \times \theta_{max}} \right)^{-1} \tag{4}$$

where c_0 is the initial value of c, A_D is the diffusion equivalent area, and $C_D(t)$ is the diffusion equivalent capacitance. A_D and $C_D(t)$ are device dependent. For the non-masking device and the Teflon-masking device, the first terms in the bracket are given by (Nair

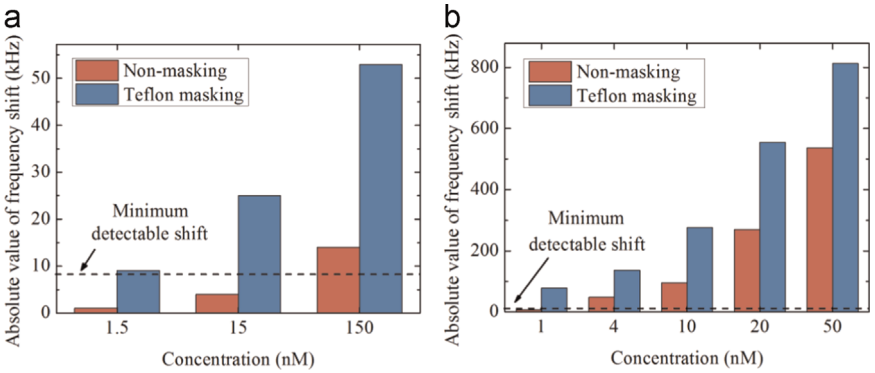

Fig. 3. Comparison of FBAR sensor signals for both (a) BSA detections at 150 nM, 15 nM, 1.5 nM, and (b) anti-IgG detections at 50 nM, 20 nM, 10 nM, 4 nM and 1 nM. The incubation time is 20 min.

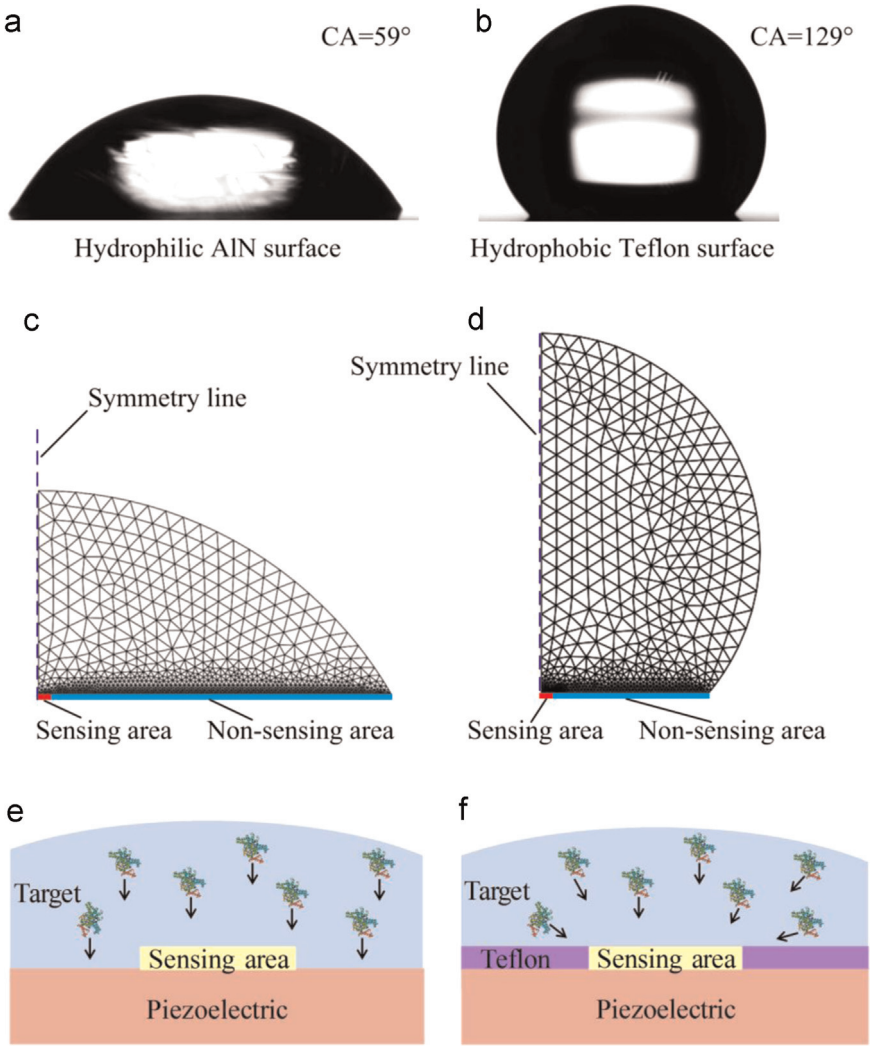

Fig. 4. Detail information used in Finite element method (FEM) simulation. The contact angles of a 4 μL DI water droplet on the surfaces of (a) bare AlN and (b) Teflon coated AlN, respectively. Geometry and meshing of the droplets are modeled with sensing area and non-sensing areas (to scale) for (c) non-masking device and (d) Teflon masking device, respectively. Two assumed diffusion schemes of target molecules: (e) a uniform-distributed diffusion in non-masking system and (f) a sensing area-centered hemispheric diffusion in a Teflon masking system.

and Alam, 2006)

$$\frac{C_D(t)}{A_D} = \frac{D}{\sqrt{2D \times t}} \tag{5}$$

and

$$\frac{C_D(t)}{A_D} = \frac{2D}{l^2\left[l^{-1} - \left(l + 2\sqrt{6D \times t}\right)^{-1}\right]} \tag{6}$$

respectively, where D is the diffusion coefficient of the target molecule and l is the length of the sensing area (i.e. sensor size). For biomolecule detections with micro or nanosensors, such as protein detections with an FBAR sensor, $2\sqrt{6D \times t}$ is typically much larger than l in practical incubation time range. For example, the former is three orders of magnitude larger than the latter, given the sensor size of 1 μm and the typical incubation time of 10 min. Therefore, Eq. (6) can approximate to a simpler form. The signal amplification ratio $\delta(t)$ by theory, which is defined by the c_s ratio of Teflon-masking device to non-masking device, can be calculated with the above approximation as

$$\delta(t) \approx \frac{\sqrt{\frac{2t}{D}} + \frac{1}{k_{on} \times \theta_{max}}}{\frac{l}{2D} + \frac{1}{k_{on} \times \theta_{max}}} \tag{7}$$

In this work, we carefully set parameters in the BSA-FBAR sensor system. D is 6×10^{-11} m^2/s, l is 1×10^{-4} m, k_{on} is 17 m^3/(mol s), and θ_{max} is 1×10^{-7} mol/m^2 (Schasfoort and Tudos, 2008). Apart from the four parameters, the signal amplification ratio $\delta(t)$ should also be a function of incubation time t.

3.3.3. Incubation time accumulated signal amplification

The analytical model is first compared with the BSA experiment data. The signal amplification ratio $\delta(t)$ by experiment is calculated as the ratio of the Teflon masking sensor signal to the non-masking sensor signal. As shown in Fig. 5a, the theoretical $\delta(t)$ by the analytical model agrees well with the results obtained by experiments in a practical time range, and all the values of signal amplification ratio greater than 1 reveal that the signals are amplified. The observed difference between the theoretical and experimental $\delta(t)$ may be attributed to the factors which were not included in the analytical model, such as nonuniform adsorption

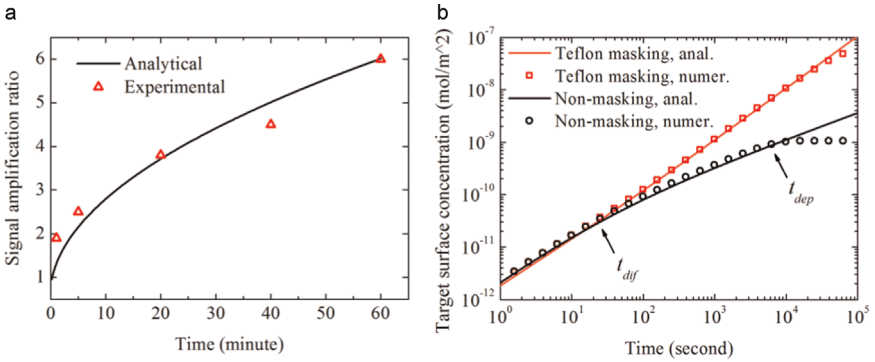

Fig. 5. Comparison results of analytical simulation, numerical simulation and experiment in BSA detections. (a) With Teflon masking FBAR sensors, both the signal amplification ratio $\delta(t)$ obtained from analytical model and experiment gradually increase along with incubation time. The BSA concentration used in the experiment is 150 nM. (b) The surface concentration of bounded target c_s calculated by analytical model shows excellent agreement with that calculated by numerical model with both the Teflon masking and non-masking sensors before t_{dep}. The analytical model is no longer valid after t_{dep}.

of the target molecules, probable multilayer receptor sites on the device surface, and unexpected target molecular adsorption on the masked region.

It should be noted that both theoretical and experimental $\delta(t)$ gradually increase as the incubation time gets longer, i.e. an accumulated signal amplification with longer incubation time. Models are employed to explore the origin of the incubation time accumulated $\delta(t)$. As Fig. 5b shows, both analytical model and numerical model predict an increasing number of adsorbed target molecules along with incubation time in a large dynamic time range.

At initial stage, the target molecules at device surface quickly adsorb to the sensing area with little diffusions, and the surface concentration of bounded target c_s increases linearly with the incubation time. The molecular adsorption rates of the masking and non-masking devices are almost the same. With the more target molecules binding on the sensor surface, a depletion zone is formed close to the absorbed area; thus the diffusion of nearby molecules to the device surface takes off. In the Teflon masking device, the depleted region is quickly supplemented by the neighboring molecules, preserved by the mask, in all directions around the sensing area and the bulk concentration c near the sensing area does not drop much. However, in the non-masking device, the depleted region can only be supplemented by the target molecules diffused from the top layer and c near the sensing area begins to drop gradually. Therefore, after a critical time node t_{dif}, target diffusion kinetics begins to dominate. c_s of the Teflon masking device remains a linear relationship with incubation time, while the non-masking device changes to a power-law relationship with an exponent of approximately 0.5. The gradual increasing deviation from t_{dif} between the two curves explains the time dependent feature of $\delta(t)$.

As the incubation time gets longer, the depletion length gets larger. The depletion-limited phase begins at another critical time node t_{dep} when the depletion reaches the droplet boundary. Since very low initial bulk concentration of target c_0 is used in simulations, the sensing area is hardly saturated with target molecules. Long time incubation with sustained adsorption depletes the molecules in the tiny droplet, and c near the sensing area decreases consequently. The numerical adsorption rate of non-masking device suffers from a sudden decrease after t_{dep}, and deviates from the analytical one. The deviation is not obvious in the Teflon masking device, since the degree of depletion is not as high as that in the non-masking ones. The deviation comes from the invalidity of analytical model after t_{dep}, since the depletion-limited phase is not considered in the model. However, t_{dep} is typically very large with microliter scale droplets, and hence the analytical model is applicable in many practical cases. t_{dep} can be roughly estimated by balancing between depletion length and the droplet radius. The depletion lengths for the non-masking and Teflon masking devices are $\sqrt{2D \times t}$ and $\sqrt{6D \times t}$, respectively (Nair and Alam, 2006). In addition, the analytical result is fairly consistent with the numerical result before t_{dep}, which basically proves the correctness of the analytical model.

3.4. Performance optimization

To fully utilize the signal amplification merit of the Teflon masking method, increasing incubation time is an obvious choice as revealed by both the simulation and experimental results. However, longer incubation time is unfavorable in many cases taking into account the tiny volume of sample droplets and it also impairs the detection efficiency. Therefore it is critical to speed up the "accumulation course" in the amplification strategy.

The device parameters may be optimized to maintain a relatively high $\delta(t)$ while restricting the incubation time to a practical range. Although the numerical model is available, the analytical model is more helpful in intuitive understanding of the mechanism and especially in device optimization. The optimization can be conducted with deducing the minimum detectable time t_0, which is the minimum time to capture a detectable signal. t_0 of the Teflon masking device is derived from Eqs. (4) and (6) as

$$t_0 = \frac{c_{s0}}{c_0} \times \left(\frac{l}{2D} + \frac{1}{k_{on} \times \theta_{max}} \right) \tag{8}$$

where c_{s0} is the minimum detectable surface concentration, which causes a minimum detectable signal of the sensor. It is obvious from Eq. (8) that t_0 can be reduced by optimizing the parameters in the bracket, where the first term determines the molecular supplement rate to the depletion region, i.e. diffusion course, and the second term determines the adsorption rate of molecules near device surface, i.e. binding course. The two courses must be accelerated simultaneously. D and K_{on} are relatively invariable in specific analyte detections, while l and θ_{max} are largely dependent on the device design and receptors surface modification conditions.

Given c_{s0} to be 1×10^{-10} mol/m^2 and c_0 to be 15 pM; t_0 is estimated by sweeping l and θ_{max}. As shown in Fig. 6, the incubation time may be reduced from several hours to an acceptable range via optimizing l and θ_{max}; meanwhile, the signal amplification effect is still effectively utilized with a Teflon masking device. The result shows that smaller sensors and appropriate surface condition of sensing area (Duan et al., 2015; Gao et al., 2012; Zheng et al., 2005) are desirable. The merit of the masking method may be further exploited by nanosensors. However, it should be noted that solely

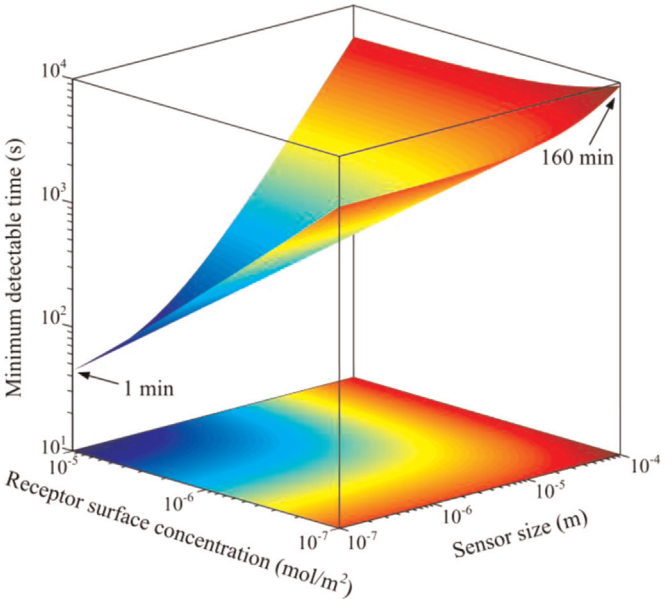

Fig. 6. The minimum detectable time t_0 (log scale) calculated by analytical model as a function of sensor size l and surface concentration of receptor sites θ_{max}, given minimum detectable surface concentration c_{s0} to be 1×10^{-10} mol/m^2 and initial bulk concentration of target c_0 to be 15 pM. t_0 can be reduced from 160 min to 1 min by optimizing l and θ_{max}.

shrinking sensor size or increasing concentration of receptor sites is not effective enough.

It should be noted that the experimental and simulation results are derived within certain conditions, i.e. limited liquid boundary and static liquid condition. The analyte is restricted in a digital droplet which is approximately stationary in this research, in contrast to a continuously flowed analyte-containing liquid (Sapsford et al., 2001), where the bulk concentration of target is always uniform in the liquid and no depletion zone will be formed near the sensor surface after target adsorption begins. Therefore, as expected and Sapsford's experimental results suggest, sensor size reduction will not help amplify the sensor signal and the analytical model is invalid in the continuously flowed liquid conditions. The analytical model is more accurate with the static liquid restriction.

Moreover, the analytical model is also applicable to the anti-IgG system, since the k_{on}/k_{off} ratio is experimentally measured to be 1×10^7 /M (obtained by BLItz System, see also Fig. S3 in Supporting information) and it is fair to conduct the approximation of Eq. (3) by taking off k_{off} (Nair and Alam, 2006) in the analytical model deduction. The analytical model can also be applied to other high binding affinity protein–ligand pairs (e.g. antibody–antigen binding systems), (Duan et al., 2012; Vacic et al., 2011) and sequence-specific DNA hybridizations.

The model gives a general insight into the kinetics of signal amplification, and will enlighten other researchers with similar questions on their biosensors.

4. Conclusion

In order to study the kinetic issues of the protein sensing with local adsorption strategy, microfabricated FBAR mass sensors with Teflon masking are successfully fabricated. The BSA physical adsorption and antibody–antigen specific binding are monitored using the prototype sensors which show that *LOD* of an FBAR biosensor is improved by more than an order of magnitude with the masking method. An analytical model is developed based on the molecule diffusions and first order binding kinetics in confined droplets. The incubation time accumulated signal amplification effect is discovered by the experiments and analytical model simultaneously. The effect is briefly explained by the analytical model, which is validated by the numerical model. The analytical model also gives guidance on the device design to make full use of the local adsorption techniques. We anticipate that the analytical model and discussion on mechanism of the signal amplification can be directly applied to a variety of micro/nano fabricated biosensors.

Acknowledgments

The authors gratefully acknowledge financial support in part from the National Natural Science Foundation of China (NSFC no. 61176106) and the 111 Project (B07014). X. Duan acknowledges support by the Tianjin Applied Basic Research and Advanced Technology (14JCYBJC41500).

Appendix A. Supplementary material

Supplementary data associated with this article can be found in the online version at http://dx.doi.org/10.1016/j.bios.2015.05.061.

References

Bunimovich, Y.L., Ge, G., Beverly, K.C., Ries, R.S., Hood, L., Heath, J.R., 2004. Langmuir 20, 10630–10638.
Choi, C.J., Belobraydich, A.R., Chan, L.L., Mathias, P.C., Cunningham, B.T., 2010. Anal. Biochem. 405, 1–10.
Duan, X., Mu, L., Sawtelle, S.D., Rajan, N.K., Han, Z., Wang, Y., Qu, H., Reed, M.A., 2015. Adv. Funct. Mater. 25, 2279–2286.
Duan, X., Li, Y., Rajan, N.K., Routenberg, D.A., Modis, Y., Reed, M.A., 2012. Nat. Nanotechnol. 7, 401–407.
Ekins, R.P., 1998. Clin. Chem. 44, 2015–2030.
Gao, A., Lu, N., Wang, Y., Dai, P., Li, T., Gao, X., Wang, Y., Fan, C., 2012. Nano Lett. 12, 5262–5268.
Georgiadis, R., Peterlinz, K.P., Peterson, A.W., 2000. J. Am. Chem. Soc. 122, 3166–3173.
Jebrail, M.J., Bartsch, M.S., Patel, K.D., 2012. Lab Chip 12, 2452–2463.
Kim, C.H., Ahn, J.H., Kim, J.Y., Choi, J.M., Park, T.J., Choi, Y.K., 2013. BioNanoScience 3, 192–197.
Kim, E., Choi, Y.K., Song, J., Lee, J., 2013a. Mater. Res. Bull. 48, 5076–5079.
Kim, J.Y., Choi, K., Moon, D.I., Ahn, J.H., Park, T.J., Lee, S.Y., Choi, Y.K., 2013b. Biosens. Bioelectron. 41, 867–870.
Lee, C.S., Lee, S.H., Park, S.S., Kim, Y.K., Kim, B.G., 2003. Biosens. Bioelectron. 18, 437–444.
Lifson, M.A., Roy, D.B., Miller, B.L., 2014. Anal. Chem. 86, 1016–1022.
Loock, H.P., Wentzell, P.D., 2012. Sens. Actuators B—Chem. 173, 157–163.
Luong, J.H.T., Male, K.B., Glennon, J.D., 2008. Biotechnol. Adv. 26, 492–500.
Malic, L., Brassard, D., Veres, T., Tabrizian, M., 2010. Lab Chip 10, 418–431.
Moulin, A.M., O'Shea, S.J., Badley, R.A., Doyle, P., Welland, M.E., 1999. Langmuir 15, 8776–8779.
Nair, P.R., Alam, M.A., 2006. Appl. Phys. Lett. 88, 233120.
Nakata, S., Kido, N., Hayashi, M., Hara, M., Sasabe, H., Sugawara, T., Matsuda, T., 1996. Biophys. Chem. 62, 63–72.
Naujoks, N., Stemmer, A., 2003. Microelectron. Eng. 67–68, 736–741.
Nirschl, M., Blüher, A., Erler, C., Katzschner, B., Vikholm-Lundin, I., Auer, S., Vörös, J., Pompe, W., Schreiter, M., Mertig, M., 2009. Sens. Actuators A—Phys. 156, 180–184.
Nirschl, M., Rantala, A., Tukkiniemi, K., Auer, S., Hellgren, A.C., Pitzer, D., Schreiter, M., Vikholm-Lundin, I., 2010. Sensors 10, 4180–4193.
Pang, W., Zhao, H., Kim, E.S., Zhang, H., Yu, H., Hu, X., 2012. Lab Chip 12, 29–44.
Park, I., Li, Z., Pisano, A.P., Williams, R.S., 2007. Nano Lett. 7, 3106–3111.
Renault, J.P., Bernard, A., Juncker, D., Michel, B., Bosshard, H.R., Delamarche, E., 2002. Angew. Chem. Int. Ed. 41, 2320–2323.
Sapsford, K.E., Liron, Z., Shubin, Y.S., Ligler, F.S., 2001. Anal. Chem. 73, 5518–5524.
Sauerbrey, G., 1959. Z. Phys. 155, 206–222.
Schasfoort, R.B.M., Tudos, A.J., 2008. Handbook of Surface Plasmon Resonance, first ed. Royal Society of Chemistry, London.
Sheehan, P.E., Whitman, L.J., 2005. Nano Lett. 5, 803–807.
Silin, V., Weetall, H., Vanderrah, D.J., 1997. J. Colloid Interface Sci. 185, 94–103.
Vacic, A., Criscione, J.M., Rajan, N.K., Stern, E., Fahmy, T.M., Reed, M.A., 2011. J. Am. Chem. Soc. 133, 13886–13889.

Whitesides, G.M., 2006. Nature 442, 368–373.
Wingqvist, G., Bjurström, J., Hellgren, A.-C., Katardjiev, I., 2007. Sens. Actuators B—Chem. 127, 248–252.
Wingqvist, G., Anderson, H., Lennartsson, C., Weissbach, T., Yantchev, V., Spetz, A.L., 2009. Biosens. Bioelectron. 24, 3387–3390.
Xie, P., Xiong, Q., Fang, Y., Qing, Q., Lieber, C.M., 2012. Nat. Nanotechnol. 7, 119–125.
Yola, M.L., Atar, N., Eren, T., 2014. Sens. Actuators B—Chem. 198, 70–76.
Zhang, H., Kim, E.S., 2005. J. Microelectromech. Syst. 14, 699–706.
Zhang, H., Marma, M.S., Kamal-Bahl, S., Kim, E.S., McKenna, C.E., 2007. IEEE Sens. J. 7, 1587–1588.
Zhang, H., Pang, W., Marma, M.S., Lee, C.Y., Kamal-Bahl, S., Kim, E.S., McKenna, C.E., 2010. Appl. Phys. Lett. 96, 123702.
Zhang, H., Jia, Z., Lv, X., Zhou, J., Chen, L., Liu, R., Ma, J., 2013. Biosens. Bioelectron. 44, 89–94.
Zhang, M., Cui, W., Chen, X., Wang, C., Pang, W., Duan, X., Zhang, D., Zhang, H., 2015. J. Micromech. Microeng. 25, 025002.
Zheng, G., Patolsky, F., Cui, Y., Wang, W.U., Lieber, C.M., 2005. Nat. Biotechnol. 23, 1294–1301.
Zhou, X., Zhang, L., Armani, A.M., Zhang, D., Duan, X., Liu, J., Zhang, H., Pang, W., 2014. IEEE J. Sel. Top. Quantum Electron. 20, 5200110.